Separation and Purification Technology 278 (2022) 119654

Contents lists available at ScienceDirect

Separation and Purification Technology

journal homepage: www.elsevier.com/locate/seppur

Equilibrium, kinetics and breakthrough curves of acetaminophen adsorption onto activated carbons from microwave-assisted $FeCl_3$-activation of lignin

A. Gómez-Avilés, M. Peñas-Garzón, C. Belver *, J.J. Rodriguez, J. Bedia *

Departamento de Ingeniería Química, Facultad de Ciencias, Universidad Autónoma de Madrid, Campus Cantoblanco, Madrid E-28049, Spain

ARTICLE INFO

Keywords:
Adsorption
$FeCl_3$ activation
Acetaminophen
Isotherms
Breakthrough curves

ABSTRACT

Activated carbons have been prepared by chemical activation of lignin with $FeCl_3$ using microwave (MW) heating. The use of MW significantly reduced the activation time compared to conventional heating. Microwave power, impregnation ratio (R: mass ratio of $FeCl_3$ to lignin precursor) and MW holding time have been studied as variables affecting the development of porous texture. The optimum conditions were found at 800 W, R = 5 and 30 min MW heating time. Under those conditions an essentially microporous activated carbon was obtained, with BET surface area higher than 1150 $m^2 \cdot g^{-1}$ and acidic surface, whose pH at the point of zero charge was 4.2. This activated carbon was tested for the adsorption of acetaminophen, as model emerging contaminant, from aqueous phase. The adsorption isotherms, obtained at 20, 40 and 60 °C, fitted well to Redlich–Peterson model. The maximum acetaminophen adsorption reached about 300 $mg \cdot g^{-1}$ at 60 °C. Values of 35.5 $kJ \cdot mol^{-1}$ and 238.3 $J \cdot mol^{-1} \cdot K^{-1}$ were obtained for the enthalpy and entropy of adsorption, respectively. Those positive values are indicative of an endothermic process and increased randomness at the solid/solution interface upon adsorption. The adsorption kinetics was better described by pseudo-second order driving force model. Breakthrough curves were also obtained at different adsorption temperatures, flow rates and acetaminophen inlet concentrations. They fitted well to a logistic-type equation representative of the Bohart-Adams, Thomas and Yoon-Nelson models. Adsorbent regeneration with hot water (80 °C) revealed easy and complete desorption thus providing a promising view of the potential application of this activated carbon.

1. Introduction

Emerging contaminants (ECs) are increasingly detected in wastewaters and water bodies. Consequently, their removal and/or degradation are receiving special attention since these compounds can produce negative effects on both environment and human health [1]. ECs include heterogeneous families of compounds, such as personal care products, pharmaceuticals, flame retardants, herbicides and other industrial chemicals. Acetaminophen is a worldwide used pain reliever and a fever reducer whose consumption is continuously growing. Worldwide production was close to 1 Mt in 2020 [2] and its detection in both the inlet and exit streams of wastewater treatment plants (WWTP) is more and more frequent [3]. The concentration of acetaminophen in water is highly dependent on the specific source of the water or wastewater considered. Taking this into account, acetaminophen has been detected in concentrations up to 10 $mg \cdot L^{-1}$ in WWTP effluents [4]. A lower concentration of 1.35 $mg \cdot L^{-1}$ was observed in hospital wastewater [5], and an average concentration of 15 $\mu g \cdot L^{-1}$ has been founded in surface water [6]. Growing research efforts are devoted to the development of cost-effective solutions for the removal of this and other contaminants of emerging concern. Among the different treatments, adsorption can be considered one of the simplest and easiest to implement, since it avoids the use of chemicals and additional steps for the recovery or treatment of possible reaction by-products.

Different materials have been tested as adsorbents for the removal of ECs, being activated carbons one of the most widely studied. Activated carbons are carbon-based materials with turbostratic structure and characterized by a well-developed porous texture, mostly in the range of microporosity. These materials are used in a diversity of applications, such as catalysis, electrochemical or energy storage and, above all, adsorption for purification of gases and liquids [7-10]. Activated carbons can be obtained from many different high-carbon content

* Corresponding author.
E-mail addresses: carolina.belver@uam.es (C. Belver), jorge.bedia@uam.es (J. Bedia).

https://doi.org/10.1016/j.seppur.2021.119654
Received 12 July 2021; Received in revised form 1 September 2021; Accepted 1 September 2021
Available online 4 September 2021

precursors, preferably with low amounts of inorganic components. These include discarded tires [11-13], coal [14-16], lignin [17-23] or various biomass wastes [24-26], among many others. Currently, the preparation of activated carbons from wastes is still of interest because it provides a way of recycling them into a value-added product, in the context of circular economy [27,28]. Activated carbons can be prepared by so-called physical and chemical activation [10,29]. This second consists basically in thermal treatment in inert atmosphere after impregnation of the starting substrate with some activating agent, most commonly $ZnCl_2$, H_3PO_4, NaOH or KOH. $FeCl_3$-activation is receiving increasing attention because of some interesting features of the resulting carbons, like a predominantly acidic surface, with a pH at the point of zero charge (pH_{PZC}) below 5.0 and the presence of remaining iron species which confer catalytic and magnetic properties, this last facilitating their separation from the liquid phase after use.

Activation uses in general conventional heating. However, it is interesting to explore some other sources and in that respect microwave (MW) is a good candidate allowing much faster and uniform heating [30,31]. As it is well known, heat transfer does not take place by conventional conduction but by dipole rotation and ionic conduction from the inner of the particles. The application of high frequency produces a fast change of the orientation of the molecules with a permanent dipole in opposite direction to the applied field. This fast and continuous synchronized change of orientation of the molecules generates a high amount of heat, resulting in enormous temperature gradient from the hot inner of the particles to their cooler surface. Thus, microwave heating requires significantly shorter time, allowing energy saving [32]. The literature contains many studies on MW-assisted preparation of activated carbons but, to the best of our knowledge, $FeCl_3$ has not been used thus far as activated agent under microwave heating.

The current work studies that activation procedure using lignin as starting feedstock and analyzes the application of the resulting activated carbon as adsorbent in aqueous phase, using acetaminophen as representative emerging contaminant. The influence of impregnation ratio and activation time on the development of porosity is investigated. The carbon with the most developed porous texture was used for the subsequent adsorption study, covering equilibrium and kinetics. Values of adsorption enthalpy and entropy have been obtained as well as the breakthrough curves. Regeneration of the activated carbon is also studied.

2. Experimental section

2.1. Materials

Lignin was provided in powder by GreenValue S.A. (Protobind™1000, Granit, Switzerland). Iron (III) chloride hexahydrate ($FeCl_3{\cdot}6H_2O$, ACS reagent, 97%), acetaminophen (analytical standard) and HCl (ACS reagent, 37%) were supplied by Sigma Aldrich.

2.2. Preparation of the activated carbons

Lignin (5 g) was physically mixed with the corresponding amount of activating agent, $FeCl_3{\cdot}6H_2O$, at different mass ratios from 1 to 5 (R = mass ratio $FeCl_3$:lignin in dry basis, d.b.). The mixture was homogenized by grinding and introduced in a quartz flask, which in turn was placed in the inner of a conventional microwave furnace (Samsung, model MG23F301TAK) with slight modifications and a maximum power of 800 W. A scheme of the experimental set-up is included in **Figure S1**. Prior to heating, a N_2 flow (150 $Ncm^3{\cdot}min^{-1}$) was passed to guarantee an inert atmosphere inside the flask. Different experiments were performed at 450, 600 and 800 W and holding times in the 5–45 min range. At MW power below 800 W no significant development of porosity was achieved and, therefore, all the results reported correspond to the activated carbons prepared at 800 W. The N_2 flow was maintained during the cooling down of the sample, which was much faster than the commonly needed after conventional heating. The resulting carbon samples were washed with an aqueous HCl (0.1 N) solution at 70 °C for 2 h and then rinsed with distilled water at room temperature up to neutral pH of the eluate. Finally, the samples were dried overnight in an oven at 60 °C. The resulting activated carbon were denoted as CR-t, being R the impregnation ratio and t the heating time in minutes (e.g. C2-30, is the activated carbon obtained using an impregnation ratio of 2 and a MW holding time of 30 min).

2.3. Characterization techniques

Elemental analyses were performed using a LECO CHNS-932 analyser to quantify the C, N, S and H contents of the samples. The porous texture was characterized by N_2 adsorption–desorption at − 196 °C using a Micromeritics TriStar II apparatus. Around 150 mg (d.b.) of the carbon were outgassed at 150 °C during at least 12 h. Brunauer-Emmett-Teller (BET) method was used to obtain the BET surface area (S_{BET}) [33]. The t-plot method was used to assess the micropore volume (V_{micro}) and the non-microporous or so-called external area (S_{EXT}) [34]. The total volume of pores (V_{pore}) was estimated from the amount (expressed as liquid) of N_2 adsorbed at 0.99 relative pressure. The pore size distribution was assessed by the density functional theory (DFT) [35]. The activated carbon with the most developed porous texture was subjected to further characterization. The morphology of the carbons prior and after adsorption was analysed with a scanning electron microscopy (SEM, Hitachi S4800, Tokyo, Japan) at an accelerating voltage of 15 kV using secondary electron (SE) and backscattered electron (BSE) detectors. The pH drift method was used to obtain the pH at the point of zero charge (pH_{PZC}). [36]. For that purpose, 50 mL of NaCl solution (0.01 M) were placed in a closed titration vessel. The pH value was adjusted from 3 to 11 using 0.1 M HCl or NaOH aqueous solutions. Next, 20 mg of activated carbon were suspended in the different solutions and bubbled with N_2 for 30 min to remove dissolved gasses. After 5 h under stirring, the final pH was measured and represented versus the initial one, the intersection of both curves corresponding to the pHpzc. X-ray photoelectron spectra (XPS) were obtained using a K-Alpha Thermo Scientific spectrometer with Al Kα (1486.7 eV) X-ray source. The C1s signal at 284.5 eV was used as reference for correcting possible changes produced by sample charging. Fourier Transform Infrared (FTIR) spectra were obtained in a Bruker iFS 66VS spectrometer in the wavenumber range of 4000–400 cm^{-1} with 2 cm^{-1} of resolution. The activated carbons were mixed with KBr and pelletized prior to the analysis.

2.4. Liquid-phase adsorption experiments

The activated carbon with the most developed porous texture was tested in the adsorption of acetaminophen from aqueous solution. In a first stage, batch equilibrium experiments were carried out at different temperatures (20, 40 and 60 °C) using 50 mL of aqueous solutions with different initial concentrations of acetaminophen in the range of 10 to 100 $mg{\cdot}L^{-1}$, with 250 $mg{\cdot}L^{-1}$ of activated carbon. After 24 h of stirring at controlled temperature in an orbital shaker at equivalent 200 rpm, the liquid phase was filtered (Whatman®, membrane filters PTFE, 0.45 μm pore size) and analysed. Kinetic adsorption tests were also performed in the same batch system with an initial acetaminophen concentration of 60 $mg{\cdot}L^{-1}$ and the same solution volume, activated carbon concentration and temperatures above mentioned for the equilibrium tests. Dynamic tests to obtain the breakthrough curves were also performed at same adsorption temperatures and acetaminophen inlet concentrations of 5, 10 and 20 $mg{\cdot}L^{-1}$. The experiments were carried out in a fixed bed (4 mm of internal diameter) in downward mode. The mass of activated carbon was always 50 mg (particle size 100 – 200 μm) with a total bed length of 15 mm. Three different flow rates were used, 1.0, 1.5 and 3.0 $mL{\cdot}min^{-1}$, corresponding to 4.8, 7.2 and 14.4 $m^3{\cdot}m^{-2}{\cdot}h^{-1}$ superficial velocity, respectively, values within the commonly operating range in full-scale liquid-phase adsorption columns.

The acetaminophen concentration was quantified by HPLC using a Shimadzu Prominence-I LC-2030C apparatus with a diode array detector (SPD-M30A) and a reverse phase C18 column (Eclipse Plus 5 μm, Agilent Technologies) at the maximum acetaminophen absorption (wavelength of 246 nm). The mobile phase consisted of a mixture of acetonitrile/acetic acid 0.1% v/v solutions, using a gradient method (10/90 to 40/60% for 17 min) with a constant flow of 0.7 mL·min^{-1}. In the dynamic tests the exit acetaminophen concentration was continuously measured in a UV–Vis spectrometer (Shimadzu UV-2600) at 246 nm wavelength, passing the outlet stream through a flow cell (model QS 10.00 mm High Precision Cell, Hellma Analytics).

3. Results and discussion

3.1. Characterization of the activated carbons

Table 1 summarizes the elemental analyses and ash content of the feedstock lignin and the resulting activated carbons, with the corresponding yield values (activated carbon to lignin mass percentage in dry basis). A deep carbonization takes place upon much shorter time than the needed in conventional heating activation of the same and other precursors and using the same activating agent [36,37]. After only 20 min of MW holding time, a carbon product with more than 90% C was obtained. Somewhat higher carbonization was observed by increasing that time within the range tested (up to 45 min) whereas varying the impregnation ratio from 1 to 3 did not show a significant effect in that respect but increased the ash content of the resulting carbon due to more residual Fe remaining after washing.

Fig. 1 displays the N_2 adsorption–desorption isotherms at − 196 °C of the activated carbons obtained at an impregnation ratio of 3 and different activation times (A) and at different impregnation ratios and an activation time of 30 min (B). Table 2 summarizes the main features relative to the porous texture. All the isotherms correspond to predominantly microporous solids with some minor contribution of mesoporosity [38] as confirmed by the low values of the external (S_{EXT}) compared to the BET surface area as well as the high micropore (V_{micro}) respect the total pore volume (V_{pore}). The lowest activation time tested (5 min) was not enough to produce some significant development of porosity but in the interval up to 10 min a dramatic change was observed leading to almost 900 $m^2 \cdot g^{-1}$ of BET surface area. Looking at the activated carbons obtained at R = 3 and different MW holding times (Fig. 1**A**) it can be seen increasingly developed porous texture up to 30 min and further decrease of the BET surface area at longer time, which may be due to some pore contraction and/or coalescence of small adjacent pores into larger ones. Regarding the effect of the impregnation ratio, the maximum textural development was achieved at the highest value tested (R = 5), with a BET surface area close to 1200 $m^2 \cdot g^{-1}$. This is higher than the reported in the literature from chemical activation of different precursors with $FeCl_3$ by conventional heating [37], except the one given by us in a previous work [30] with Tara gum (1600 $m^2 \cdot g^{-1}$). With lignin as precursor we achieved a maximum surface area of 818 $m^2 \cdot g^{-1}$ [39], about 70 % of the one reached in the current work. Therefore, these results support the benefits of using MW heating instead of conventional sources in chemical activation. A higher contribution of mesoporosity was also associated to the use of higher impregnation ratio within the range tested, in agreement with the behaviour observed when using other activating agents (e.g., H_3PO_4 and $ZnCl_2$) under conventional heating.

Table 1
Elemental analyses (d.a.f.), ash content (d.b.) and yield values (d.b.)

	%C	%H	%N	%O*	Ash (%)	Yield (%)
Lignin	61.6	6.0	1.1	29.3	2.0	–
C3-5	70.1	2.4	0.9	22.9	3.7	80.9
C3-10	87.7	1.0	1.2	5.9	5.2	56.2
C3-20	90.4	1.5	1.1	3.2	5.8	53.0
C3-30	92.2	0.8	0.9	2.0	5.9	51.2
C3-45	93.3	0.4	0.6	1.4	6.4	48.4
C1-30	92.5	1.2	1.3	1.8	5.8	42.1
C5-30	91.3	1.2	1	2.3	6.9	54.8

* by difference; d.a.f (dry ash-free); d.b. (dry basis)

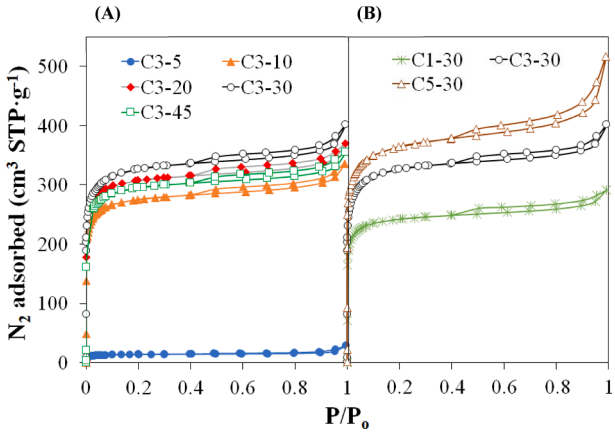

Fig. 1. N_2 adsorption–desorption isotherms at − 196 °C of the activated carbons obtained at an impregnation ratio of 3 and different activation times (A) and at different impregnation ratios and an activation time of 30 min (B).

Table 2
Summary of the porous texture of the activated carbons.

	S_{BET} ($m^2 \cdot g^{-1}$)	S_{EXT} ($m^2 \cdot g^{-1}$)	V_{micro} ($cm^3 \cdot g^{-1}$)	V_{pore} ($cm^3 \cdot g^{-1}$)
C3-5	44	4	0.02	0.04
C3-10	888	50	0.41	0.52
C3-20	982	45	0.46	0.58
C3-30	1052	49	0.49	0.63
C3-45	898	42	0.45	0.56
C1-30	738	38	0.36	0.37
C5-30	1177	95	0.53	0.66

The pore size distributions of the activated carbons, as obtained by the DFT method, are depicted in Fig. 2. All of them show mainly unimodal pore size distributions, with mean pore sizes between 10 and 12 Å, although there are also pores with mean sizes around 16 and even 18–19 Å in much lower amounts. Some small differences can be observed depending on the activation time. The activated carbon prepared at 30 min show somewhat narrower microporosity whereas at higher time some widening of the micropores takes place (Fig. 2**A**). Regarding the effect of impregnation ratio, narrower microporosity is

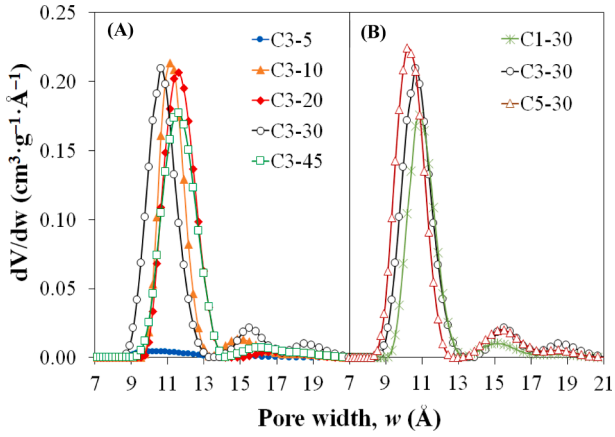

Fig. 2. Pore size distributions of activated carbons obtained at an impregnation ratio of 3 and different activation times (A) and at different impregnation ratios and an activation time of 30 min (B).

associated to a higher R value (Fig. 2**B**).

Besides the porous texture, surface chemistry plays an important role in adsorption. To learn on the surface chemistry of the activated carbons, FTIR and XPS profiles of these materials were obtained, as well as the pH at the point of zero charge. FTIR spectra of the carbon samples obtained at different activation times and R = 3 can be seen in **Figure S2**, accompanied of a brief discussion. The most important feature is the transition occurring in the interval of 5 to 10 min activation time, with a strong loss of surface chemical groups, confirming deep carbonization beyond that time.

The deconvoluted XPS profiles of C5-30 carbon (the one with the most developed porous texture) are shown in **Figures S3** (C 1 s and O 1 s, both with a brief explanation) and Fig. 3 (Fe 2p), as representative example. The Fe 2p XPS spectrum (Fig. 3) was deconvoluted in a doublet related to Fe $2p_{3/2}$ and Fe $2p_{1/2}$ contributions, with a quantified separation between them of 13.6 eV [40]. The spectrum was deconvoluted with a main Fe $2p_{3/2}$ peak at around 711.2 eV, with the corresponding Fe $2p_{1/2}$ contribution at 724.8 eV, characteristic of Fe^{3+} species, thus corroborating the presence of iron oxides in the surface. These peaks are accompanied by a lower satellite peak at around 718.1 eV.

Fig. 4**A and B** represent SEM images of the activated carbon C5-30 prior adsorption using secondary electron (SE) and backscattered electron (BSE) detectors, respectively. The activated carbon shows a very irregular surface completely covered of holes and craters with thin walls randomly distributed along the solid, most likely produced by the loss of organic volatile matter occurred during the fast activation process. The BSE image (Fig. 4**B**) clearly shows the presence of homogeneously distributed crystals, which may be iron oxide crystals (as observed by XPS) strongly attached to the carbon since they were not removed during the acid washing step performed after the microwave activation. We have also obtained SEM images of C5-30 after adsorption (**Figure S4**). No changes are observed neither on the carbon surface nor in the distribution of the iron oxide particles.

Fig. 5 shows the plots for the determination of the pH_{PZC} of the carbons prepared at 30 min activation time and the three impregnation ratios tested. In all cases the pH_{PZC} value was 4.2. Therefore, these activated carbons will become negatively charged in aqueous solutions of higher pH than that value, as a consequence of deprotonation of functional surface groups [41]. Acetaminophen behaves as a weak acid with a pK_a of 9.38, and thus at pH below the pK_a the molecules are predominantly in its neutral form (see speciation diagram in **Figure S5**). In the current study we performed all the adsorption tests at natural pH (values varied between 6.3 and 7.2). In these conditions, the activated carbon surface will be negatively charged while acetaminophen will be in molecular form (uncharged) and, therefore, adsorption must not be determined by electrostatic attraction, in agreement with the observed in previous studies [42,43].

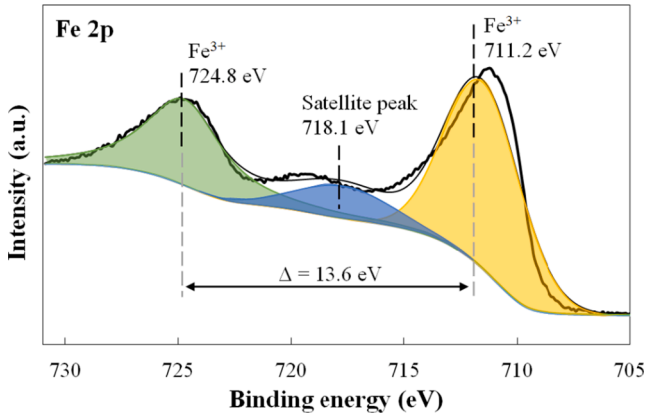

Fig. 3. Fe 2p XPS deconvoluted spectrum of C5-30 activated carbon.

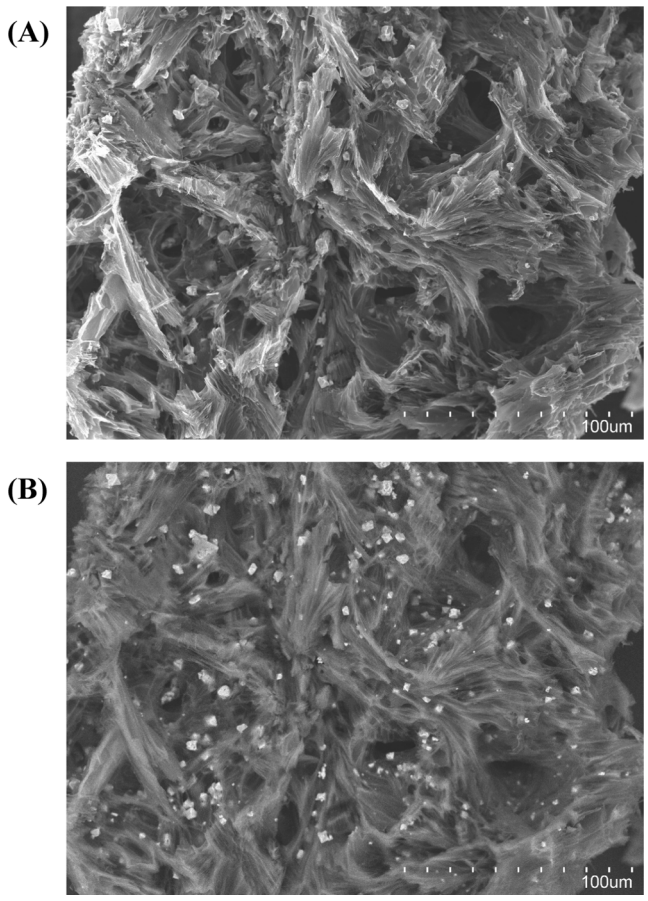

Fig. 4. SEM images of the activated carbon C5-30 prior adsorption using secondary electron (A) and backscattered electron (B) detectors.

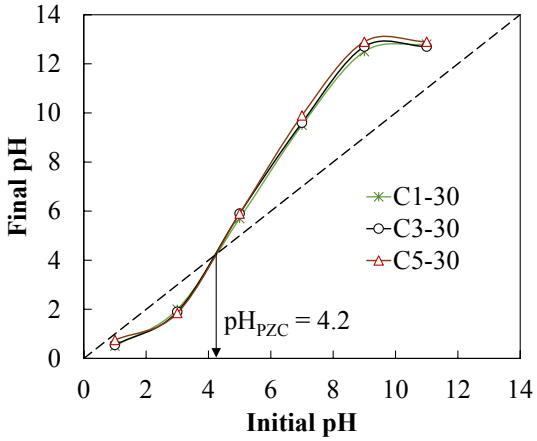

Fig. 5. pH at the point of zero charge (pH_{PZC}) of the carbons prepared at 30 min of activation time.

3.2. Adsorption equilibrium and thermodynamics

Since C5-30 showed the most developed porous texture it was selected for the adsorption tests. Fig. 6 depicts the acetaminophen equilibrium adsorption isotherms at 20, 40 and 60 °C onto C5-30. They can be classified as L type of Giles classification [44], quite common in liquid-phase adsorption, with strong adsorbate-adsorbent attractive forces and weak interactions between the adsorbate molecules themselves. Remarkably, the amount adsorbed at equilibrium increases with

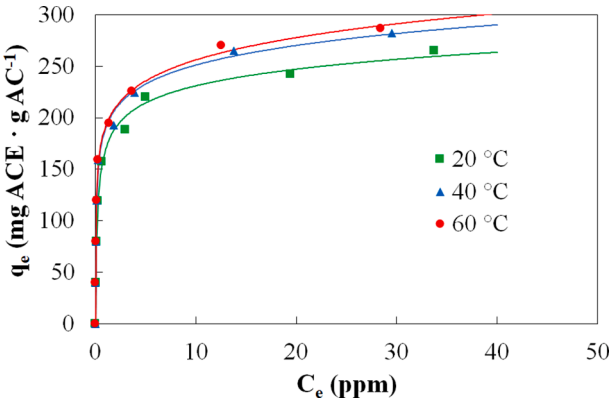

Fig. 6. Acetaminophen equilibrium adsorption at different temperatures onto C5-30 (C_o = 10 – 100 mg ACE·L^{-1}; w = 250 mg·L^{-1}). Experimental points and fitting curves to Redlich–Peterson isotherm model.

temperature, being that more pronounced in the 20–40 °C range. This trend, opposite to what occurs in physical adsorption, is in agreement with the previously reported by Galhetas et al. [45] for the adsorption of acetaminophen onto activated carbons from partial gasification (physical activation) of pine residues. However, García-Mateos et al. [46] observed the opposite with an activated carbon from chemical activation of olive stones with H_3PO_4, as well as Moussavi et al. with double-oxidized graphene oxide [47]. These discrepancies may be explained by a determining specific role of the surface chemistry of the adsorbent. However, this was discarded by Galhetas et al. [48], who observed opposite behaviours in carbons with similar surface acidity and concluded that microporosity should be the main factor ruling out the adsorption trend with temperature [45].

We have obtained a maximum acetaminophen adsorption capacity close to 300 mg·g^{-1}, this value is significantly higher than those reported in the literature for other activated carbons and other types of adsorbents, although it should be considered that the differences in the adsorption conditions make difficult a direct comparison of the adsorbent performances. In this sense, Kerkhoff et al. [49] reported a significantly lower acetaminophen adsorption capacity of 100 mg·g^{-1} with a zinc chloride activated carbon from *Butia capitata* endocarp. We have also obtained a much lower adsorption capacity (120 mg·g^{-1}) of acetaminophen when using an organo-sepiolite adsorbent [50]. Yanyan et al. [51] analysed the fixed bed adsorption on low-cost coconut shell waste achieving a maximum adsorption capacity of 38 mg·g^{-1}. Nguyen et al. [43] reported a Langmuir maximum adsorption capacity of 221 mg·g^{-1} using a commercial activated carbon and initial concentration of acetaminophen in the 100 – 1200 mg·L^{-1} range, significantly higher than the used in our study. Many more studies reported lower adsorption capacities than that herein reported. A slightly higher adsorption capacity (330 mg·g^{-1}) was achieved by Spessato et al. [52] with an activated carbon produced by carbonization and chemical activation with potassium hydroxide pellets of grains of Jatoba fruits. It should be remarked that the activated carbon obtained has a very high surface area (c.a. 2800 m^2·g^{-1}), but a much longer synthesis time is needed (2 h or carbonization plus 2 h of activation, versus 30 min in our case). A much higher Langmuir adsorption capacity (704 mg·g^{-1}) was obtained by Moussavi et al. [47] although with a more complex adsorbent based on double-oxidized graphene oxide.

The experimental adsorption isotherms were fitted to different models. Table 3 summarizes the corresponding equations, the values obtained for the fitting parameters and the correlation coefficient (R^2), together with the corresponding equations. In addition to the most commonly used two-parameters models (Freundlich [53] and Langmuir [54]) several three-parameters isotherms (Sips [55], Redlich-Peterson [56] and Toth [57]) were checked. These last provided very good fitting whereas the frequently used in liquid phase adsorption,

Table 3
Adsorption isotherms fitting.

Model	Mathematical expression	Values of the parameters	R^2
Freundlich	$q_e = K_F \cdot C_e^n$	20 °C K_F = 143.87; n = 0.188	0.970
		40 °C K_F = 163.82; n = 0.179	0.976
		60 °C K_F = 171.36; n = 0.173	0.982
Langmuir	$q_e = \frac{q_L \cdot K_L \cdot C_e}{1 + K_L \cdot C_e}$	20 °C q_L = 238.80; K_L = 3.75	0.983
		40 °C q_L = 250.66; K_L = 7.02	0.979
		60 °C q_L = 251.56; K_L = 8.96	0.972
Sips	$q_e = \frac{q_S \cdot (K_S \cdot C_e)^n}{1 + (K_S \cdot C_e)^n}$	20 °C q_S = 272.64; K_S = 2.08; n = 0.61	0.991
		40 °C q_S = 306.80; K_S = 2.56; n = 0.50	0.991
		60 °C q_S = 328.90; K_S = 2.29; n = 0.43	0.996
Redlich–Peterson	$q_e = \frac{q_{RP} \cdot K_{RP} \cdot C_e}{1 + (K_{RP} \cdot C_e)^n}$	20 °C q_{RP} = 159.44; K_{RP} = 8.80; n = 0.91	0.996
		40 °C q_{RP} = 146.68; K_{RP} = 22.97; n = 0.90	0.997
		60 °C q_{RP} = 126.12; K_{RP} = 50.54; n = 0.89	0.999
Toth	$q_e = \frac{q_T \cdot K_T \cdot C_e}{[1 + (K_T \cdot C_e)^n]^{1/n}}$	20 °C q_T = 283.31; K_T = 11.79; n = 0.49	0.993
		40 °C q_T = 326.11; K_T = 56.13; n = 0.37	0.993
		60 °C q_T = 364.29; K_T = 224.59; n = 0.29	0.997

q_e (mg·g^{-1}) is the amount of acetaminophen adsorbed at equilibrium; C_e (mg·L^{-1}) is the solute concentration at equilibrium; K_F (mg·g^{-1})/(mg·L^{-1})^n is the Freundlich constant; n (dimensionless) is the model exponent; q_L (mg·g^{-1}) is the Langmuir adsorption capacity; K_L (L·mg^{-1}) is the Langmuir constant; q_S (mg·g^{-1}) is the Sips adsorption capacity; K_S (L·mg^{-1}) is the Sips constant; q_{RP} (mg·g^{-1}) is the Redlich–Peterson adsorption capacity; K_{RP} (L·mg^{-1}) is the Redlich–Peterson constant; q_T (mg·g^{-1}) is the Toth adsorption capacity; K_T (L·mg^{-1}) is the Toth constant.

Freundlich and Langmuir, showed higher deviations, specially the second, since the ideal assumptions of preferential monolayer coverage and energetic homogeneity of adsorption sites must be unlikely. Fig. 6 depicts the fitting curves of Redlich-Peterson model, the one that better described the experimental equilibrium data. The remaining are included as supplementary information (**Figure S6**).

The free energy (ΔG), enthalpy (ΔH) and entropy (ΔS) of adsorption were calculated from the following well-known expressions:

$$\Delta G = -R \cdot T \cdot \ln(K_{RP})$$

$$\Delta G = \Delta H - T \cdot \Delta S$$

The free energy values obtained were –34.3, –39.1 and –43.9 kJ·mol^{-1} at 20, 40 and 60 °C, respectively, indicating spontaneous process as in most practical cases of liquid phase adsorption. Fitting the ln(K_{RP}) versus 1/T values allows obtaining the enthalpy and entropy of adsorption by simple linear regression (**Figure S7**). These values were 35.5. kJ·mol^{-1} and 238.3 J·mol^{-1}·K^{-1}, respectively. The endothermic character of this adsorption process but with low ΔH absolute value is compatible with predominantly physical and/or low-strength chemical adsorption. Meanwhile, the positive value of adsorption entropy suggests an increase of the randomness at the solid/solution interface. It is well-known that acetaminophen can form different oligomers, mainly dimers, in liquid phase [58,59]. In this sense, we have previously confirmed the presence of these dimers when analysing the photodegradation pathway of acetaminophen [60,61]. Therefore, the increase of disorder accompanying adsorption could be explained by the breakdown of dimers resulting in a dissociative adsorption mechanism [62].

3.3. Adsorption kinetics

Fig. 7 shows the kinetic curves of acetaminophen adsorption onto C5-30 at different temperatures. Adsorption proceeds quite fast, and the rate does not seem to be significantly affected by temperature within the range tested. Several models have been used in the literature to describe the adsorption kinetics [63,64]. In this study, we have checked some of the most common, namely pseudo-first order, pseudo-second order, intraparticle diffusion and Elovich. Table 4 summarizes the corresponding equations and the values obtained for the characteristic parameters by non-liner fitting. The correlation coefficients are also given. The driving force-based pseudo-second order model provided the best fitting, depicted in Fig. 7 (for the remaining models checked see **Figure S8**). The Elovich model yielded also fairly good fitting, while the pseudo-first order can be useful for the early stages [65] and the intraparticle diffusion model showed significant discrepancies with the experimental results. For this model to be applicable, the value of the C parameter should be close to zero, otherwise intraparticle diffusion is not likely the rate-limiting step.

The activated carbon dosage can greatly affect the adsorption process. **Figure S9A** represents the acetaminophen adsorbed amount versus the adsorption time at activated carbon dosages between 50 and 250 $mg{\cdot}L^{-1}$. The increase of the adsorbent dosage seems to reduce the adsorption capacity of the activated carbon. This behaviour can be due to the higher availability of vacant adsorption sites at higher adsorbent dosages. The concentration of acetaminophen is constant, but the number of adsorption sites increases with the activated carbon dosage and, consequently, not all the sites of the active carbon are occupied. We have also analysed the effect of the presence of some common ions in the adsorption kinetics (**Figure S9B**). The presence of Cl^-, NO_3^-, $SO_4^=$ and HCO_3^- ions seems to have a very limited effect on the adsorption process, only a low-significant reduction can be observed. This agrees with the non-electrostatic adsorption of acetaminophen molecules. The change of the water matrix from distilled to tap water reduces more significantly the amount adsorbed. This should be a consequence of the competitive adsorption of the substances present in the tap water with the acetaminophen molecules, resulting in a slight decrease of the acetaminophen adsorption capacity of the activated carbon.

3.4. Adsorption dynamics: Fixed bed tests

Fig. 8 shows the breakthrough curves of acetaminophen adsorption onto C5-30 at different temperatures, flow rates (or the corresponding superficial velocity) and inlet concentrations. The breakthrough time increases with temperature (Fig. 8**A**) consistently with the already seen increase of the adsorption capacity. The total bed adsorption capacities

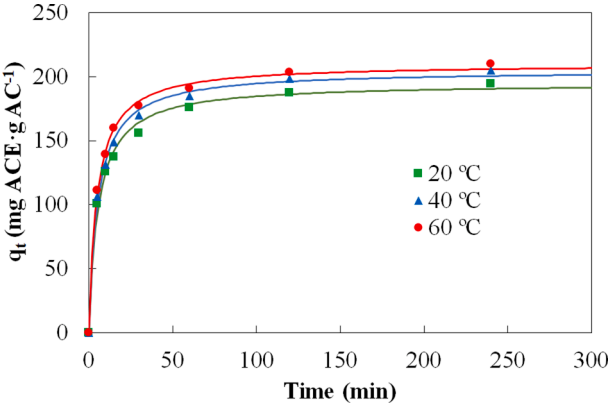

Fig. 7. Kinetic curves of acetaminophen adsorption onto C5-30 at different temperatures ($[ACE]_o$ = 60 $mg{\cdot}L^{-1}$; V = 50 mL; w = 250 $mg{\cdot}L^{-1}$). Symbols: Experimental points; Lines: Fitting to pseudo-second order model.

Table 4
Fitting of the experimental kinetic adsorption data.

Model	Mathematical expression	Values of the parameters	R^2
Pseudo-first order	$q_t = q_e{\cdot}(1- e^{-k_1{\cdot}t})$	20 °C q_e = 178.58; k_1 = 0.124	0.979
		40 °C q_e = 189.65; k_1 = 0.124	0.984
		60 °C q_e = 195.27; k_1 = 0.135	0.987
Pseudo-second order	$q_t = \frac{k_2{\cdot}q_e^2{\cdot}t}{1 + k_2{\cdot}q_e{\cdot}t}$	20 °C q_e = 193.02; k_2 = $9.645{\cdot}10^{-4}$	0.997
		40 °C q_e = 193.02; k_2 = $9.645{\cdot}10^{-4}$	0.998
		60 °C q_e = 193.02; k_2 = $9.645{\cdot}10^{-4}$	0.999
Intraparticle diffusion	$q_t = k_p{\cdot}\sqrt{t} + C$	20 °C k_p = 10.219; C = 72.047	0.822
		40 °C k_p = 10.722; C = 77.368	0.814
		60 °C k_p = 10.785; C = 83.046	0.800
Elovich	$q_t = \frac{1}{\beta}{\cdot}\ln(1 + \alpha{\cdot}\beta{\cdot}t)$	20 °C α = 392.16; β = 0.041	0.996
		40 °C α = 457.31; β = 0.039	0.995
		60 °C α = 691.92; β = 0.040	0.993

q_t ($mg{\cdot}g^{-1}$) is the amount of acetaminophen adsorbed at a specific time; q_e ($mg{\cdot}g^{-1}$) is the amount of acetaminophen adsorbed at equilibrium; t (min) is the adsorption time; k_1 (min^{-1}) is the pseudo-first order model rate constant; k_2 ($g{\cdot}mg^{-1}{\cdot}min^{-1}$) is the pseudo-second order model rate constant; k_p ($mg{\cdot}g^{-1}{\cdot}min^{-0.5}$) is the rate constant of the intraparticle diffusion model; C ($mg{\cdot}g^{-1}$) is a constant related to the thickness of the boundary layer; α ($mg{\cdot}g^{-1}{\cdot}min^{-1}$) is the Elovich initial rate constant; β ($mg{\cdot}g^{-1}$) is the desorption constant.

were obtained by numerical integration of the area above the breakthrough curve up to $C/C_o = 1$. The resulting values were 217, 245 and 265 $mg{\cdot}g^{-1}$ at 20, 40 and 60 °C, respectively. As expected, increasing the flow rate reduces the breakthrough time (Fig. 8**B**), but the liquid volume passed through the bed up to the breaking point (taken at $C/C_0 = 0.05$) is almost the same and the length of the mass transfer zone does not vary significantly with the flow rate within the range tested, indicating that there are no limitations by external diffusion. The calculated total bed adsorption capacities were quite similar (213, 217 and 215 $mg{\cdot}g^{-1}$ at 60, 90 and 180 $mL{\cdot}h^{-1}$, respectively), which supports the consistency of the breakthrough curves. Finally, in Fig. 8**C**, can be seen how increasing the inlet concentration of acetaminophen decreases the breakthrough time and increases the total bed adsorption capacities (207, 217 and 245 $mg{\cdot}g^{-1}$ at 5, 10 and 20 $mg{\cdot}L^{-1}$, respectively), in agreement with the equilibrium uptakes at those concentrations.

The breakthrough curves were fitted to a logistic growth function:

$$\frac{C}{C_o} = \frac{1}{1 + e^{(a-b{\cdot}t)}}$$

being a (dimensionless) and b (min^{-1}) the two adjustable parameters. This function is mathematically compatible with three commonly used simplistic models of fixed bed dynamics, namely Bohart-Adams [66], Thomas [67] and Yoon-Nelson [68], as recently reviewed by Chu [69]. The corresponding expressions are shown below:

$$\text{Bohart-Ad.} \ln\left(\frac{C_o}{C} - 1\right) = \frac{k_{BA}{\cdot}N_o{\cdot}L}{u} - k_{BA}{\cdot}C_o{\cdot}t$$

$$\text{Thomas} \ln\left(\frac{C_o}{C} - 1\right) = \frac{k_T{\cdot}q_o{\cdot}M}{Q} - k_T{\cdot}C_o{\cdot}t$$

$$\text{Yoon} - \text{Nelson} \ln\left(\frac{C_o}{C} - 1\right) = k_{YN}{\cdot}\tau - k_{YN}{\cdot}t$$

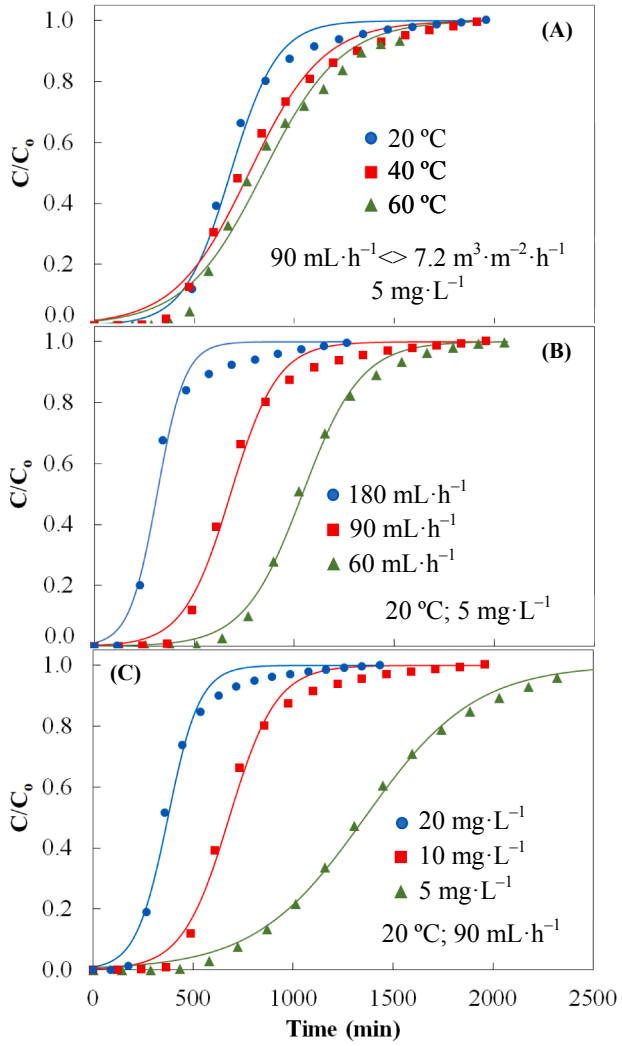

Fig. 8. Breakthrough curves of acetaminophen adsorption onto C5-30 at different conditions. Symbols: Experimental points; Lines: model fitting.

where k_{BA} ($cm^3 \cdot mg^{-1} \cdot min^{-1}$) is the Bohart-Adams rate coefficient, N_o ($mg \cdot cm^{-3}$) the adsorption capacity per unit volume of the bed, L the bed length (cm), and u the superficial velocity ($cm \cdot min^{-1}$). In the Thomas model, k_T ($cm^3 \cdot mg^{-1} \cdot min^{-1}$) is the Tomas rate coefficient, q_o ($mg \cdot g^{-1}$) corresponds to the adsorbate loading per unit mass of adsorbent ($mg \cdot g^{-1}$), M is the adsorbent mass (g) and Q the volumetric flow rate ($cm^3 \cdot min^{-1}$). In the Yoon-Nelson, k_{YN} is the Yoon-Nelson rate coefficient (min^{-1}) and τ (min) the time at $C/C_o = 0.5$ of the breakthrough curve. The comparison of the model equations with that of the logistic function allows stablishing the relations between a and b and the models' parameters [69], as summarized in **Table S1**. The values of those parameters are collected in Table 5. As can be seen in Fig. 8, the models fit well the experimental results (see the values of R^2 in Table 5).

3.5. Adsorbent regeneration

Regeneration of the adsorbent bed saturated at 20 °C, 90 $mL \cdot h^{-1}$ and 20 $mg \cdot L^{-1}$ inlet concentration was performed with pure water at 80 °C. Once no acetaminophen was observed in the outlet stream, another adsorption test was carried out under the same conditions than the previous one. Fig. 9 depicts the corresponding breakthrough curves, which, as can be seen, are almost coincident. The calculated amounts of acetaminophen adsorbed at complete bed saturation were 238 and 241 $mg \cdot g^{-1}$ in the first and second adsorption cycle, respectively, so that complete regeneration was achieved.

4. Conclusions

Activated carbons were prepared for the first time by chemical activation of lignin with $FeCl_3$ using microwave heating. A predominantly microporous carbon product with high BET surface area (up to 1150 $m^2 \cdot g^{-1}$) was obtained. This activated carbon was tested as adsorbent in aqueous phase using acetaminophen as model emerging pollutant. The Redlich-Petersen model provided the best fitting of the experimental equilibrium results. From the thermodynamic analysis it was determined that the adsorption process was spontaneous, endothermic and with an increase of disorder that could be associated to the breakdown of the acetaminophen dimers resulting in a dissociative adsorption mechanism. The saturation adsorption capacity reached almost 300 $mg \cdot g^{-1}$ at 60 °C. The adsorption kinetics followed a pseudo-second order model. Breakthrough curves were obtained at different temperatures, flow rates (or superficial velocities) and acetaminophen inlet concentrations. They were fitted to a logistic function representative of the Bohart-Adams, Thomas and Yoon-Nelson models. Complete

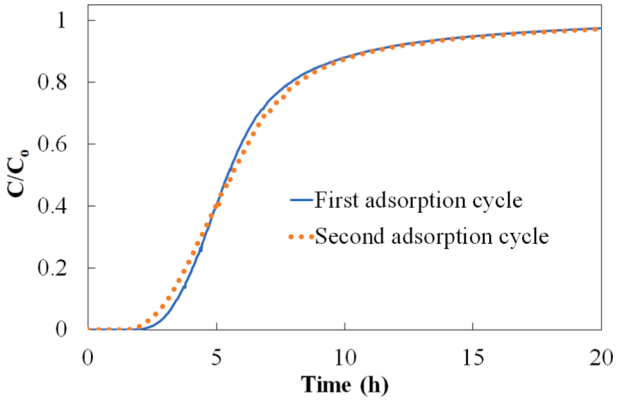

Fig. 9. Breakthrough curves from two successive adsorption cycles (20 °C, 90 $mL \cdot h^{-1}$ and 20 $mg \cdot L^{-1}$) with intermediate bed regeneration by water at 80 °C.

Table 5
Parameters of the models and correlation coefficients for the different breakthrough tests.

Test conditions			Model parameters								R^2
T (°C)	Flow rate ($mL \cdot h^{-1}$)	Co ($mg \cdot L^{-1}$)	Logistic		Bohart-Adams		Thomas		Yoon-Nelson		
			a	b	k_{BA}	N_o	k_T	q_o	k_{YN}	τ	
20	90	10	5.78	0.0085	0.85	54.1	0.85	204	0.0085	679	0.997
40	90	10	4.16	0.0054	0.54	61.5	0.54	232	0.0054	773	0.996
60	90	10	4.31	0.0051	0.51	67.0	0.51	253	0.0051	842	0.992
20	60	10	7.12	0.0068	0.69	55.2	0.69	208	0.0068	1040	0.999
20	180	10	4.48	0.0143	1.43	49.7	1.43	188	0.0143	313	0.993
20	90	5	4.92	0.0036	0.72	54.1	0.72	204	0.0036	1359	0.999
20	90	20	4.66	0.0125	0.63	59.3	0.63	224	0.0125	372	0.997

a (dimensionless); b (min^{-1}); k_{BA} ($cm^3 \cdot mg^{-1} \cdot min^{-1}$); N_o ($mg \cdot cm^{-3}$); k_T ($cm^3 \cdot mg^{-1} \cdot min^{-1}$); q_o ($mg \cdot g^{-1}$); k_{YN} (min^{-1}); τ (min)

regeneration of the adsorbent was achieved with water at 80 °C.

CRediT authorship contribution statement

A. Gómez-Avilés: Methodology, Writing – original draft. **M. Peñas-Garzón:** Methodology, Writing – original draft. **C. Belver:** Conceptualization, Writing – review & editing, Supervision, Funding acquisition. **J.J. Rodriguez:** Conceptualization, Writing – review & editing, Supervision, Funding acquisition. **J. Bedia:** Conceptualization, Writing – review & editing, Supervision, Funding acquisition.

Declaration of Competing Interest

The authors declare that they have no known competing financial interests or personal relationships that could have appeared to influence the work reported in this paper.

Acknowledgements

The authors acknowledge the financial support from the State Research Agency (PID2019-106186RB-I00/AEI/10.13039/501100011033, Spain). M. Peñas-Garzón thanks Spanish MECD for FPU16/00576 grant. Thanks to the SAIUEx service for the acquisition of the SEM images.

Appendix A. Supplementary material

Supplementary data to this article can be found online at https://doi.org/10.1016/j.seppur.2021.119654.

References

[1] O.M. Rodriguez-Narvaez, J.M. Peralta-Hernandez, A. Goonetilleke, E.R. Bandala, Treatment technologies for emerging contaminants in water: A review, Chem. Eng. J. 323 (2017) 361–380, https://doi.org/10.1016/j.cej.2017.04.106.
[2] Global Acetaminophen Market Set for Rapid Growth, (n.d.). https://www.marketresearchstore.com/news/global-acetaminophen-paracetamol-market-148 (accessed May 29, 2021).
[3] B. Petrie, R. Barden, B. Kasprzyk-Hordern, A review on emerging contaminants in wastewaters and the environment: Current knowledge, understudied areas and recommendations for future monitoring, Water Res. 72 (2015) 3–27, https://doi.org/10.1016/j.watres.2014.08.053.
[4] M.O. Chijioke-Okere, Z. Adlan Mohd Hir, C.E. Ogukwe, P.C. Njoku, A.H. Abdullah, E.E. Oguzie, TiO_2/Polyethersulphone films for photocatalytic degradation of acetaminophen in aqueous solution, J. Mol. Liq. 338 (2021) 116692, https://doi.org/10.1016/j.molliq.2021.116692.
[5] S. Ahmadzadeh, M. Dolatabadi, Removal of acetaminophen from hospital wastewater using electro-Fenton process, Environ. Earth Sci. 772 (77) (2018) 1–11, https://doi.org/10.1007/S12665-017-7203-7.
[6] A.-C. Lin, Y.-T. Tsai, Occurrence of pharmaceuticals in Taiwan's surface waters: Impact of waste streams from hospitals and pharmaceutical production facilities, Sci. Total Environ. 407 (12) (2009) 3793–3802, https://doi.org/10.1016/j.scitotenv.2009.03.009.
[7] F. Çeçen, Ö. Aktaş, Activated Carbon for Water and Wastewater Treatment: Integration of Adsorption and Biological Treatment, Wiley-VCH, Weinheim, Germany (2011), https://doi.org/10.1002/9783527639441.
[8] R.C. Bansal, M. Goyal, Activated carbon adsorption, CRC Press (2005), https://doi.org/10.1680/bwtse.63341.147.
[9] J. Rouquerol, F. Rouquerol, P. Llewellyn, G. Maurin, K.S.W. Sing, Adsorption by Powders and Porous Solids: Principles, Methodology and Applications: Second Edition, Elsevier Inc., 2013. doi:10.1016/C2010-0-66232-8.
[10] H. Marsh, F. Rodríguez-Reinoso, Activated Carbon, Elsevier Ltd (2006), https://doi.org/10.1016/B978-0-08-044463-5.X5013-4.
[11] B. Acevedo, C. Barriocanal, I. Lupul, G. Gryglewicz, Properties and performance of mesoporous activated carbons from scrap tyres, bituminous wastes and coal, Fuel. 151 (2015) 83–90, https://doi.org/10.1016/j.fuel.2015.01.010.
[12] V.K. Gupta, A. Nayak, S. Agarwal, I. Tyagi, Potential of activated carbon from waste rubber tire for the adsorption of phenolics: Effect of pre-treatment conditions, J. Colloid Interface Sci. 417 (2014) 420–430, https://doi.org/10.1016/j.jcis.2013.11.067.
[13] A.M. Ramírez-Arias, J.C. Moreno-Piraján, L. Giraldo, Adsorption of Triton X-100 in aqueous solution on activated carbon obtained from waste tires for wastewater decontamination, Adsorption. 26 (2) (2020) 303–316, https://doi.org/10.1007/s10450-019-00157-8.
[14] K. Labus, S. Gryglewicz, J. Machnikowski, Granular KOH-activated carbons from coal-based cokes and their CO_2 adsorption capacity, Fuel. 118 (2014) 9–15, https://doi.org/10.1016/j.fuel.2013.10.042.
[15] P. Chingombe, B. Saha, R.J. Wakeman, Surface modification and characterisation of a coal-based activated carbon, Carbon N. Y. 43 (15) (2005) 3132–3143, https://doi.org/10.1016/j.carbon.2005.06.021.
[16] A. Bagreev, J. Angel Menendez, I. Dukhno, Y. Tarasenko, T.J. Bandosz, Bituminous coal-based activated carbons modified with nitrogen as adsorbents of hydrogen sulfide, Carbon N. Y. 42 (3) (2004) 469–476, https://doi.org/10.1016/j.carbon.2003.10.042.
[17] J.M. Rosas, R. Ruiz-Rosas, J. Rodríguez-Mirasol, T. Cordero, Kinetic study of SO_2 removal over lignin-based activated carbon, Chem. Eng. J. 307 (2017) 707–721, https://doi.org/10.1016/j.cej.2016.08.111.
[18] L.M. Cotoruelo, M.D. Marqués, F.J. Díaz, J. Rodríguez-Mirasol, J.J. Rodríguez, T. Cordero, Adsorbent ability of lignin-based activated carbons for the removal of p-nitrophenol from aqueous solutions, Chem. Eng. J. 184 (2012) 176–183, https://doi.org/10.1016/j.cej.2012.01.026.
[19] J. Rodríguez-Mirasol, J. Bedia, T. Cordero, J.J. Rodríguez, Influence of water vapor on the adsorption of VOCs on lignin-based activated carbons, Sep. Sci. Technol. 40 (15) (2005) 3113–3135, https://doi.org/10.1080/01496390500385277.
[20] J.J. Rodríguez, T. Cordero, J. Rodríguez-Mirasol, Carbon Materials from Lignin and Their Applications, in: Prod. Biofuels Chem. from Lignin, Springer, 2016: pp. 217–262. doi:10.1007/978-981-10-1965-4_8.
[21] X. Wang, X. Chen, A. Thomas, X. Fu, M. Antonietti, Metal-Containing Carbon Nitride Compounds: A New Functional Organic-Metal Hybrid Material, Adv. Mater. 21 (16) (2009) 1609–1612, https://doi.org/10.1002/adma.v21:1610.1002/adma.200802627.
[22] X. Wang, X. Li, L. Peng, S. Han, C. Hao, C. Jiang, H. Wang, X. Fan, Effective removal of heavy metals from water using porous lignin-based adsorbents, Chemosphere. 279 (2021) 130504, https://doi.org/10.1016/j.chemosphere.2021.130504.
[23] C. Jiang, X. Wang, B. Hou, C. Hao, X. Li, J. Wu, Construction of a Lignosulfonate-Lysine Hydrogel for the Adsorption of Heavy Metal Ions, J. Agric. Food Chem. 68 (10) (2020) 3050–3060, https://doi.org/10.1021/acs.jafc.9b0754010.1021/acs.jafc.9b07540.s001.
[24] Y. Shen, Y. Zhou, Y. Fu, N. Zhang, Activated carbons synthesized from unaltered and pelletized biomass wastes for bio-tar adsorption in different phases, Renew. Energy. 146 (2020) 1700–1709, https://doi.org/10.1016/j.renene.2019.07.167.
[25] T.-H. Liou, Development of mesoporous structure and high adsorption capacity of biomass-based activated carbon by phosphoric acid and zinc chloride activation, Chem. Eng. J. 158 (2) (2010) 129–142, https://doi.org/10.1016/j.cej.2009.12.016.
[26] J.M. Rosas, J. Bedia, J. Rodríguez-Mirasol, T. Cordero, Preparation of Hemp-Derived Activated Carbon Monoliths. Adsorption of Water Vapor, Ind. Eng. Chem. Res. 47 (4) (2008) 1288–1296, https://doi.org/10.1021/ie070924w.
[27] O. Ioannidou, A. Zabaniotou, Agricultural residues as precursors for activated carbon production—A review, Renew. Sustain. Energy Rev. 11 (9) (2007) 1966–2005, https://doi.org/10.1016/j.rser.2006.03.013.
[28] J.M. Dias, M.C.M. Alvim-Ferraz, M.F. Almeida, J. Rivera-Utrilla, M. Sánchez-Polo, Waste materials for activated carbon preparation and its use in aqueous-phase treatment: A review, J. Environ. Manage. 85 (4) (2007) 833–846, https://doi.org/10.1016/j.jenvman.2007.07.031.
[29] J. Bedia, M. Peñas-Garzón, A. Gómez-Avilés, J. Rodriguez, C. Belver, A Review on the Synthesis and Characterization of Biomass-Derived Carbons for Adsorption of Emerging Contaminants from Water, C. 4 (2018) 63, https://doi.org/10.3390/c4040063.
[30] H. Deng, L.e. Yang, G. Tao, J. Dai, Preparation and characterization of activated carbon from cotton stalk by microwave assisted chemical activation-Application in methylene blue adsorption from aqueous solution, J. Hazard. Mater. 166 (2-3) (2009) 1514–1521, https://doi.org/10.1016/j.jhazmat.2008.12.080.
[31] P.S. Thue, M.A. Adebayo, E.C. Lima, J.M. Sieliechi, F.M. Machado, G.L. Dotto, J.C.P. Vaghetti, S.L.P. Dias, Preparation, characterization and application of microwave-assisted activated carbons from wood chips for removal of phenol from aqueous solution, J. Mol. Liq. 223 (2016) 1067–1080, https://doi.org/10.1016/j.molliq.2016.09.032.
[32] K. Yang, J. Peng, C. Srinivasakannan, L. Zhang, H. Xia, X. Duan, Preparation of high surface area activated carbon from coconut shells using microwave heating, Bioresour. Technol. 101 (15) (2010) 6163–6169, https://doi.org/10.1016/j.biortech.2010.03.001.
[33] S. Brunauer, P.H. Emmett, E. Teller, Adsorption of Gases in Multimolecular Layers, J. Am. Chem. Soc. 60 (2) (1938) 309–319, https://doi.org/10.1021/ja01269a023.
[34] B. Lippens, Studies on pore systems in catalysts V. The t method, J. Catal. 4 (3) (1965) 319–323, https://doi.org/10.1016/0021-9517(65)90307-6.
[35] J. Jagiello, C. Ania, J.B. Parra, C. Cook, Dual gas analysis of microporous carbons using 2D-NLDFT heterogeneous surface model and combined adsorption data of N_2 and CO_2, Carbon N. Y. 91 (2015) 330–337, https://doi.org/10.1016/j.carbon.2015.05.004.
[36] M.V. Lopez-Ramon, F. Stoeckli, C. Moreno-Castilla, F. Carrasco-Marin, On the characterization of acidic and basic surface sites on carbons by various techniques, Carbon N. Y. 37 (8) (1999) 1215–1221, https://doi.org/10.1016/S0008-6223(98)00317-0.
[37] J. Bedia, M. Peñas-Garzón, A. Gómez-Avilés, J.J. Rodriguez, C. Belver, Review on Activated Carbons by Chemical Activation with $FeCl_3$, C —, J. Carbon Res. 6 (2020) 21, https://doi.org/10.3390/c6020021.
[38] M. Thommes, K. Kaneko, A.V. Neimark, J.P. Olivier, F. Rodriguez-Reinoso, J. Rouquerol, K.S.W. Sing, Physisorption of gases, with special reference to the

evaluation of surface area and pore size distribution (IUPAC Technical Report), Pure Appl. Chem. 87 (2015) 1051–1069, https://doi.org/10.1515/pac-2014-1117.
[39] J.A. Zazo, J. Bedia, C.M. Fierro, G. Pliego, J.A. Casas, J.J. Rodriguez, Highly stable Fe on activated carbon catalysts for CWPO upon $FeCl_3$ activation of lignin from black liquors, Catal. Today. 187 (1) (2012) 115–121, https://doi.org/10.1016/j.cattod.2011.10.003.
[40] J.F. Moulder, W.F. Stickle, P.E. Sobol, K.D. Bomben, Handbook of X-Ray Photoelectron Spectroscopy, Eden Prairie, MN, Perkin-Elmer, 1992, p. 2002.
[41] J.A. Menéndez, M.J. Illán-Gómez, C.A.L. y León, L.R. Radovic, On the difference between the isoelectric point and the point of zero charge of carbons, Carbon N. Y. 33 (11) (1995) 1655–1657, https://doi.org/10.1016/0008-6223(95)96817-R.
[42] H. Nourmoradi, K.F. Moghadam, A. Jafari, B. Kamarehie, Removal of acetaminophen and ibuprofen from aqueous solutions by activated carbon derived from *Quercus Brantii* (Oak) acorn as a low-cost biosorbent, J. Environ. Chem. Eng. 6 (6) (2018) 6807–6815, https://doi.org/10.1016/j.jece:2018.10.047.
[43] D.T. Nguyen, H.N. Tran, R.-S. Juang, N.D. Dat, F. Tomul, A. Ivanets, S.H. Woo, A. Hosseini-Bandegharaei, V.P. Nguyen, H.-P. Chao, Adsorption process and mechanism of acetaminophen onto commercial activated carbon, J. Environ. Chem. Eng. 8 (6) (2020) 104408, https://doi.org/10.1016/j.jece:2020.104408.
[44] C.H. Giles, D. Smith, A. Huitson, A general treatment and classification of the solute adsorption isotherm. I. Theoretical, J. Colloid Interface Sci. 47 (3) (1974) 755–765, https://doi.org/10.1016/0021-9797(74)90252-5.
[45] M. Galhetas, A.S. Mestre, M.L. Pinto, I. Gulyurtlu, H. Lopes, A.P. Carvalho, Carbon-based materials prepared from pine gasification residues for acetaminophen adsorption, Chem. Eng. J. 240 (2014) 344–351, https://doi.org/10.1016/j.cej.2013.11.067.
[46] F.J. García-Mateos, R. Ruiz-Rosas, M.D. Marqués, L.M. Cotoruelo, J. Rodríguez-Mirasol, T. Cordero, Removal of paracetamol on biomass-derived activated carbon: Modeling the fixed bed breakthrough curves using batch adsorption experiments, Chem. Eng. J. 279 (2015) 18–30, https://doi.org/10.1016/j.cej.2015.04.144.
[47] G. Moussavi, Z. Hossaini, M. Pourakbar, High-rate adsorption of acetaminophen from the contaminated water onto double-oxidized graphene oxide, Chem. Eng. J. 287 (2016) 665–673, https://doi.org/10.1016/j.cej.2015.11.025.
[48] M. Galhetas, M.A. Andrade, A.S. Mestre, E. Kangni-foli, M.J. Villa de Brito, M. L. Pinto, H. Lopes, A.P. Carvalho, The influence of the textural properties of activated carbons on acetaminophen adsorption at different temperatures, Phys. Chem. Chem. Phys. 17 (18) (2015) 12340–12349, https://doi.org/10.1039/C4CP05273K.
[49] C.M. Kerkhoff, K.d. Boit Martinello, D.S.P. Franco, M.S. Netto, J. Georgin, E. L. Foletto, D.G.A. Piccilli, L.F.O. Silva, G.L. Dotto, Adsorption of ketoprofen and paracetamol and treatment of a synthetic mixture by novel porous carbon derived from *Butia capitata* endocarp, J. Mol. Liq. 339 (2021) 117184, https://doi.org/10.1016/j.molliq.2021.117184.
[50] A. Gómez-Avilés, L. Sellaoui, M. Badawi, A. Bonilla-Petriciolet, J. Bedia, C. Belver, Simultaneous adsorption of acetaminophen, diclofenac and tetracycline by organo-sepiolite: Experiments and statistical physics modelling, Chem. Eng. J. 404 (2021) 126601, https://doi.org/10.1016/j.cej.2020.126601.
[51] L. Yanyan, T.A. Kurniawan, M. Zhu, T. Ouyang, R. Avtar, M.H. Dzarfan Othman, B. T. Mohammad, A.B. Albadarin, Removal of acetaminophen from synthetic wastewater in a fixed-bed column adsorption using low-cost coconut shell waste pretreated with NaOH, HNO_3, ozone, and/or chitosan, J. Environ. Manage. 226 (2018) 365–376, https://doi.org/10.1016/j.jenvman.2018.08.032.
[52] L. Spessato, K.C. Bedin, A.L. Cazetta, I.P.A.F. Souza, V.A. Duarte, L.H.S. Crespo, M. C. Silva, R.M. Pontes, V.C. Almeida, KOH-super activated carbon from biomass waste: Insights into the paracetamol adsorption mechanism and thermal regeneration cycles, J. Hazard. Mater. 371 (2019) 499–505, https://doi.org/10.1016/j.jhazmat.2019.02.102.
[53] H. Freundlich, Über die Adsorption in Lösungen, Zeitschrift Für Phys. Chemie. 57 (1906) 385–471, https://doi.org/10.1515/zpch-1907-5723.
[54] I. Langmuir, The adsorption of gases on plane surfaces of glass, mica and platinum, J. Am. Chem. Soc. 40 (9) (1918) 1361–1403, https://doi.org/10.1021/ja02242a004.
[55] R. Sips, On the structure of a catalyst surface, J. Chem. Phys. 16 (5) (1948) 490–495, https://doi.org/10.1063/1.1746922.
[56] O. Redlich, D.L. Peterson, A useful adsorption isotherm, J. Phys. Chem. 63 (1959) 1024, https://doi.org/10.1021/j150576a611.
[57] Tóth, J., State Equation of the Solid-Gas Interface Layers, Acta Chim. Hung. 69 (1971) 311–328. https://ci.nii.ac.jp/naid/10017154947 (accessed June 3, 2021).
[58] D. Nematollahi, H. Shayani-Jam, M. Alimoradi, S. Niroomand, Electrochemical oxidation of acetaminophen in aqueous solutions: Kinetic evaluation of hydrolysis, hydroxylation and dimerization processes, Electrochim. Acta. 54 (28) (2009) 7407–7415, https://doi.org/10.1016/j.electacta.2009.07.077.
[59] D.W. Potter, D.W. Miller, J.A. Hinson, Identification of acetaminophen polymerization products catalyzed by horseradish peroxidase, J. Biol. Chem. 260 (22) (1985) 12174–12180, https://doi.org/10.1016/S0021-9258(17)39003-8.
[60] M. Peñas-Garzón, A. Gómez-Avilés, C. Belver, J.J. Rodriguez, J. Bedia, Degradation pathways of emerging contaminants using TiO_2-activated carbon heterostructures in aqueous solution under simulated solar light, Chem. Eng. J. 392 (2020) 124867, https://doi.org/10.1016/j.cej.2020.124867.
[61] V. Muelas-Ramos, C. Belver, J.J. Rodriguez, J. Bedia, Synthesis of noble metal-decorated NH_2-MIL-125 titanium MOF for the photocatalytic degradation of acetaminophen under solar irradiation, Sep. Purif. Technol. 272 (2021) 118896, https://doi.org/10.1016/j.seppur.2021.118896.
[62] P. Saha, S. Chowdhury, Insight Into Adsorption Thermodynamics, in: Thermodynamics, InTech, 2011: pp. 349–364. doi:10.5772/13474.
[63] J. Wang, X. Guo, Adsorption kinetic models: Physical meanings, applications, and solving methods, J. Hazard. Mater. 390 (2020) 122156, https://doi.org/10.1016/j.jhazmat.2020.122156.
[64] C. Jiang, X. Wang, G. Wang, C. Hao, X. Li, T. Li, Adsorption performance of a polysaccharide composite hydrogel based on crosslinked glucan/chitosan for heavy metal ions, Compos. Part B Eng. 169 (2019) 45–54, https://doi.org/10.1016/J.COMPOSITESB.2019.03.082.
[65] Y.S. Ho, G. McKay, A Comparison of chemisorption kinetic models applied to pollutant removal on various sorbents, Process Saf. Environ. Prot. 76 (4) (1998) 332–340, https://doi.org/10.1205/095758298529696.
[66] G.S. Bohart, E.Q. Adams, Some aspects of the behavior of charcoal with respect to chlorine, J. Am. Chem. Soc. 42 (1920) 523–544, https://doi.org/10.1021/ja01448a018.
[67] H.C. Thomas, Heterogeneous Ion Exchange in a Flowing System, J. Am. Chem. Soc. 66 (10) (1944) 1664–1666, https://doi.org/10.1021/ja01238a017.
[68] Young.Hee. Yoon, James.H. Nelson, Application of Gas Adsorption Kinetics I. A Theoretical Model for Respirator Cartridge Service Life, Am. Ind. Hyg. Assoc. J. 45 (8) (1984) 509–516, https://doi.org/10.1080/15298668491400197.
[69] K.H. Chu, Breakthrough curve analysis by simplistic models of fixed bed adsorption: In defense of the century-old Bohart-Adams model, Chem. Eng. J. 380 (2020) 122513, https://doi.org/10.1016/j.cej.2019.122513.